

Texture and microstructure of HPT-processed Fe-based shape memory alloys

R Chulist¹, M Czerny¹, A Panigrahi², M Zehetbauer², N Schell³ and W Skrotzki⁴

¹ Instytut Metalurgii i Inżynierii Materiałowej Polskiej Akademii Nauk, PL-30-059 Krakow, Poland

² Physik Nanostrukturierter Materialien, Universität Wien, A-1090 Wien, Austria

³ Institut für Werkstofforschung, Helmholtz-Zentrum Geesthacht, D-21502 Geesthacht, Germany

⁴ Institut für Festkörper- und Materialphysik, Fakultät für Physik, Technische Universität Dresden, D-01062 Dresden, Germany

E-mail: r.chulist@imim.pl

Abstract. Texture and microstructure evolution of Fe-based shape memory alloys subjected to high pressure torsion (HPT) at room temperature was investigated using synchrotron radiation and electron backscatter diffraction in the scanning electron microscope. As starting material for HPT a directionally solidified Fe-based alloy characterized by a $\langle 100 \rangle$ fiber texture and coarse columnar grains with a mean size of about 300 μm was used. Prior to HPT the samples were quenched and heat treated for precipitation hardening for 24 h at 700°C. HPT-processing changes the initial texture to a typical shear texture with dominating C component. As deformation proceeds an intensive stress-induced precipitation of a brittle NiAl-B2 phase takes place. The precipitates form a typical shear texture of *bcc* metals with F component dominating. The C and F components may lead to specific interphase orientation relationships.

1. Introduction

Fe-based alloys belong to a new family of shape memory alloys (SMAs) showing a large superelastic strain at room temperature [1, 2]. The superelastic effect is due to thermoelastic transformation of γ to α' . The alloy with a composition of Fe-28Ni-17Co-11.5Al-0.5Ta-0.05B (in at.%, abbreviated NCATB) with a strong $\{035\}\langle 100 \rangle$ recrystallization texture obtained by rolling and a special thermomechanical treatment shows a superelastic strain up to 13.5% in tensile deformation [1]. The essential prerequisite for achieving large superelastic strains in this system is precipitation hardening with size of precipitates less than 15 nm [1-16]. The main strengthening component of these alloys is the *fcc* phase with composition given by the formula $(\text{Ni}, \text{Fe}, \text{Co})_3(\text{Al}, \text{Ta})$ [10-16]. The boron addition promotes formation of the coherent Ni_3Al -type phase. On the other hand, a small amount of B is added in order to suppress grain boundary precipitation of the brittle and incoherent NiAl-B2 type phase [17].

The superelastic strain has also been observed for NCATB and FeNiCoAlTa (NCAT) single crystals, however, with smaller strain values than those reported for their polycrystalline counterparts [3]. Most recently, an abnormal high reversible strain of 15.3% for FeNiCoAlNb single crystal was observed at 77 K in tension [15]. This value was higher than the theoretical one resulting from the theory of martensite formation. The authors explain it with an unusual reversible twinning mode. Nevertheless, both FeNiCoAl-based single crystals and polycrystals are very promising for the alternative refrigeration concept based on a giant entropy change associated with the diffusionless martensitic transformation.

As a unique property of SMA, superelastic strain, can be considered as a deformation mode activated only along certain crystallographic planes and directions. Therefore, it is strongly anisotropic and directly related with the crystallographic orientation or texture. Depending on various deformation processes different textures can be obtained. Therefore, in order to change the texture, which can



drastically change the superelastic properties, high pressure torsion (HPT) processing was applied. In torsion the deformation mode is simple shear, with the amount of shear strain changing along the sample radius from zero at the center to a maximum at the edge of the disc. This allows investigating the influence of different shear strains and strain rates even on one and the same sample. As this kind of severe plastic deformation produces a submicro/nanocrystalline microstructure with a pronounced texture its application leads to properties differing from those of conventional materials. Therefore, to study the effect of HPT on texture and microstructure formation as well as precipitation hardening, the NCATB alloys were investigated using synchrotron radiation and electron backscatter diffraction in the scanning electron microscope.

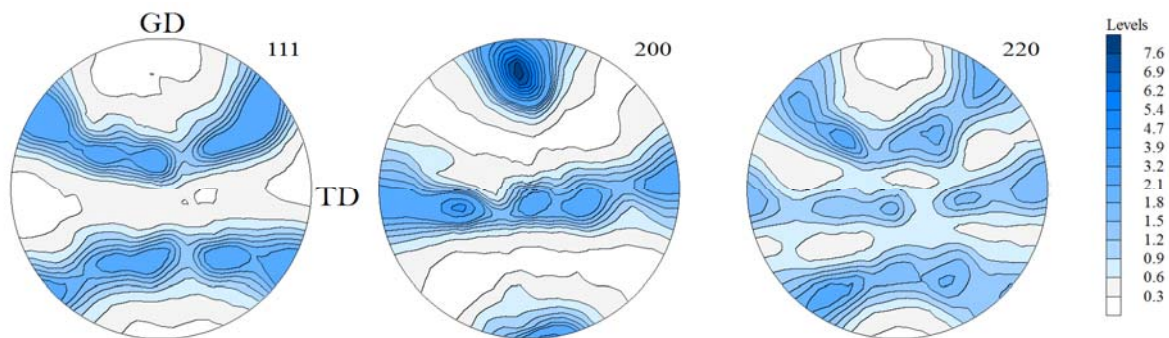


Fig. 1: $\{111\}$, $\{200\}$ and $\{220\}$ pole figures showing an initial $\langle 100 \rangle$ fiber texture. (GD = growth direction).

2. Experimental

The starting material for HPT-processing was as-cast material with Fe-28Ni-17Co-11.5Al-2.5Ta-0.05B composition [1, 4]. Before deformation the alloy was subjected to thermal hardening with rapid cooling and subsequent annealing for 24 h at 973 K [1]. From the initial ingot 3 small discs with a diameter of 8 mm and a height of 0.8 mm were cut by spark erosion. Cutting alignment was done in such a way that the growth direction (GD) was parallel to the normal direction Y of the disc. Subsequently, the discs were deformed at room temperature by HPT up to 0.25, 1 and 2 rotations at a constant pressure of 8 GPa. The texture of the HPT-processed material was measured by diffraction of high-energy synchrotron radiation (87.1 keV) using the HZG materials science beamline P07B at DESY in Hamburg, Germany [18, 19]. A pin of size 1.0 mm \times 0.8 mm \times 8 mm was cut from each sample along the radial direction for local synchrotron measurements. Such prepared samples were transmitted with synchrotron radiation with a beam size of 0.7 \times 0.7 mm along the radial direction starting at the middle of the pin. The shear strain value given corresponds to the middle of the respective analyzed volume. The experimental pole figures were calculated using StressTexCalculator software [20]. The orientation distribution function (ODF) was determined from the measured pole figures $\{111\}$, $\{200\}$, $\{220\}$ for austenite and $\{110\}$, $\{200\}$, $\{211\}$, $\{224\}$ for NiAl-B2 type precipitates using LABOTEX software [21]. To account best for the monoclinic symmetry of simple shear, the crystal and sample reference systems are defined as X \parallel shear direction (SD), Y \parallel shear plane normal (SPN), and Z \parallel transverse direction (TD) [22]. The textures are represented by $\varphi_2 = 0^\circ$ and $\varphi_2 = 45^\circ$ ODF sections, which for face- and body-centered cubic (*fcc* and *bcc*) metals contain all major shear components. After deformation the samples were investigated by scanning electron microscopy and EBSD in order to reveal the microstructure evolution of the NCATB alloys.

3. Results and discussion

The initial cast sample was characterized by long columnar grains with an average size of about 300 μm . The matrix (austenite) had a strong $\langle 100 \rangle$ fiber texture along GD, Fig. 1 [23]. Fig. 2 shows EBSD maps taken from the initial material and samples after HPT achieving shear strains of 1.96, 3.92, 7.84

and 15.68. As can be seen, with increasing shear strain the grains become more elongated. Shear deformation changes the shape of the austenitic grains from about equiaxed to elliptical with the long axis oriented towards SD.

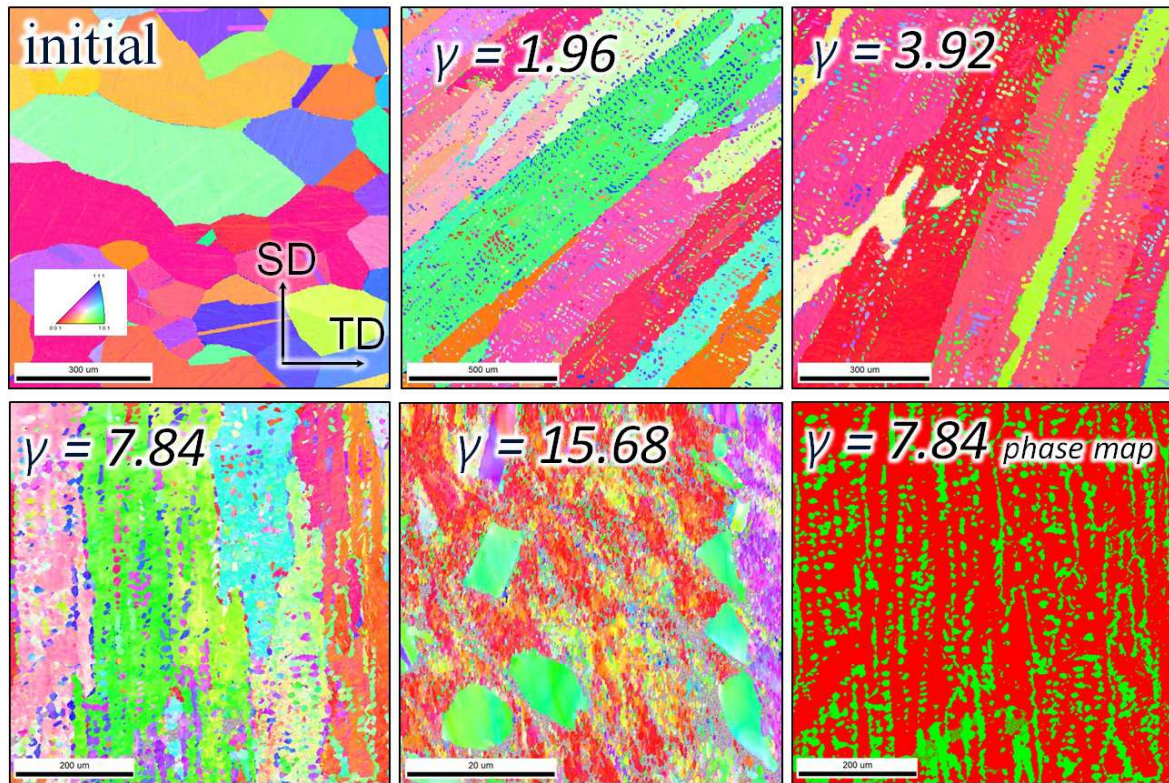


Fig. 2: EBSD maps of the initial NCATB material and subjected to HPT at different shear strains. The phase map shows austenite (red) and NiAl-B2 phase (green) for $\gamma = 7.84$.

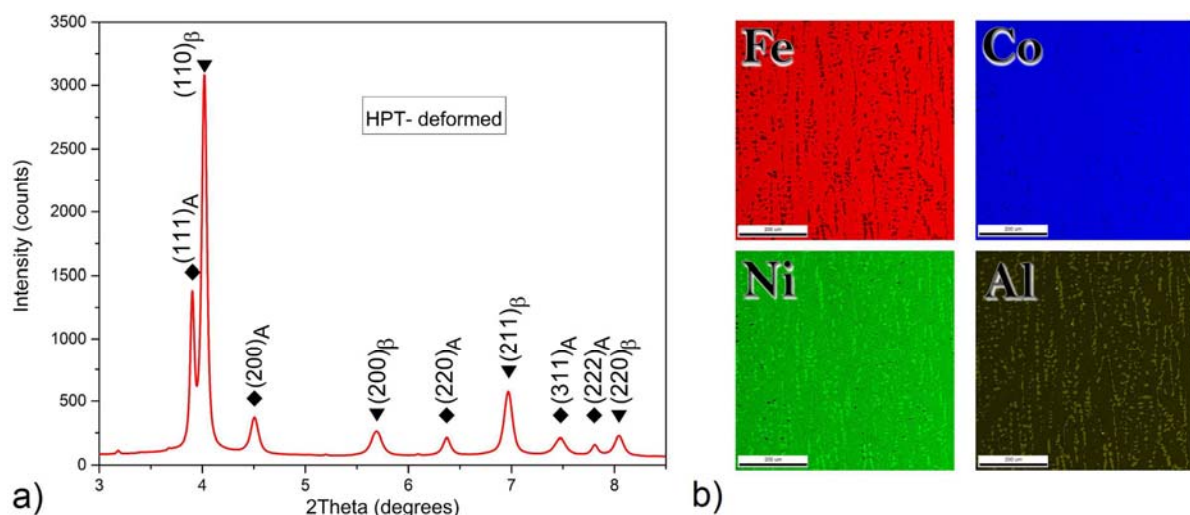


Fig. 3: (a) Diffractogram taken with synchrotron radiation of NCATB alloy deformed by HPT at a shear strain of 15.68 (A – austenite, β – NiAl-B2 phase). (b) EDS maps show the distribution of four main elements Fe, Co, Ni, Al.

Additionally, HPT leads to an intensive precipitation process promoting the NiAl-B2 type intermetallic phase. The high amount of NiAl-B2 phase can be clearly seen in one of the X-ray diffractograms given in Fig. 3a which was used for texture measurements. The same holds for the EDS maps given in Fig. 3b where almost an equal distribution of Ni and Al is unveiled in all precipitates.

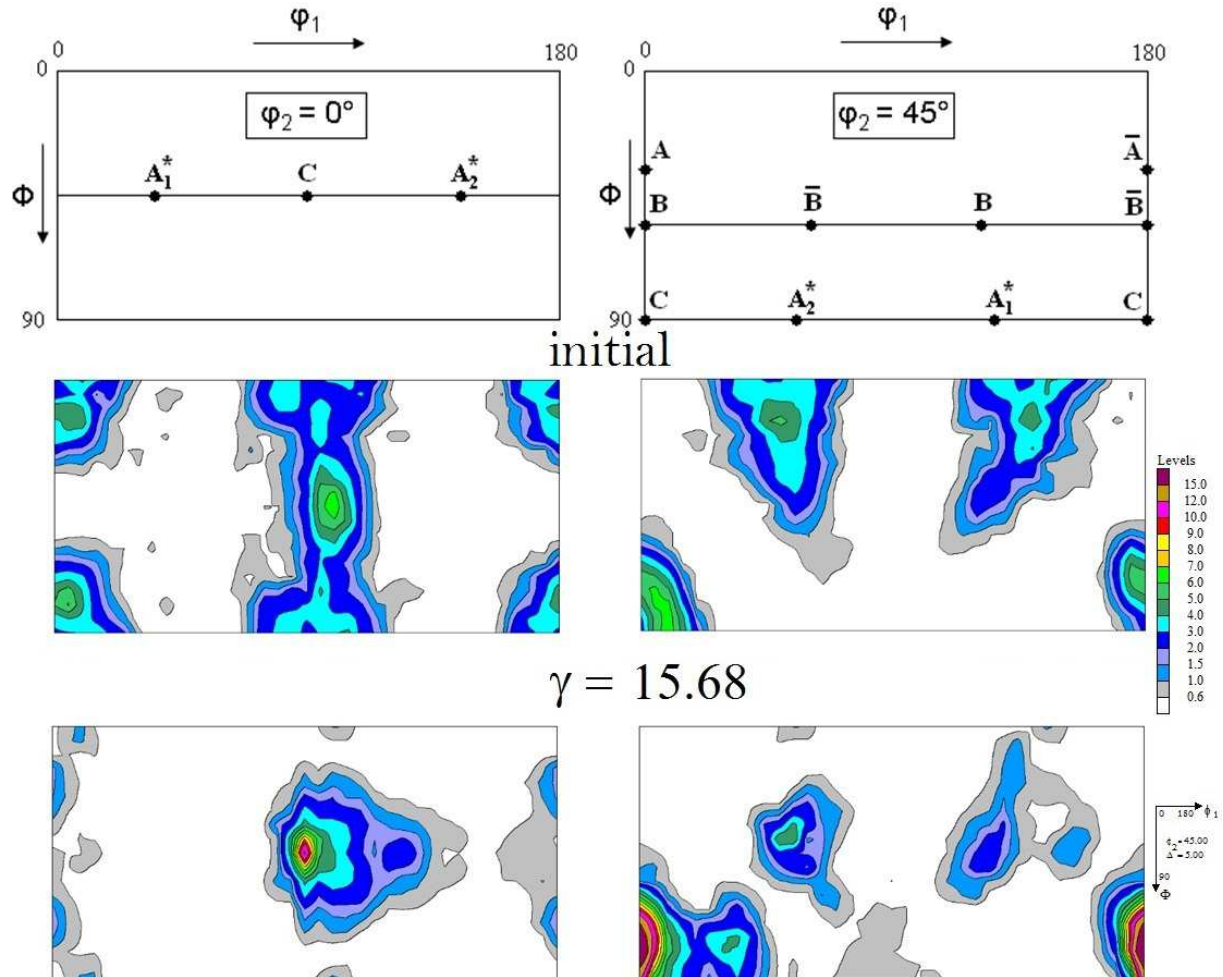


Fig. 4: ODF sections at $\varphi_2 = 0^\circ$ and 45° of the initial cast sample and after HPT at a shear strain of 15.68 for austenite phase. Key figures give the ideal components of simple shear of *fcc* metals. Intensities are given in multiples of random distribution (mrd).

The HPT process changes the initial fiber texture of the austenitic phase (denoted as A) to a shear texture with typical simple shear components for *fcc* metals with strong $C = \{100\}\langle 110 \rangle$ ({plane parallel shear plane}<direction parallel SD>), Fig. 4. The C component is typical for simple shear of *fcc* metals with high stacking fault energy and may also be promoted by the initial $\langle 100 \rangle$ fiber texture. Moreover, HPT performed at room temperature generates a massive precipitation of the NiAl-B2 phase. With increasing shear the volume fraction of this phase increases up to about 31%. Fig. 5 exhibits the ODF sections at $\varphi_2 = 0^\circ$ and 45° which clearly show that the shear deformation of particles causes a typical shear texture for *bcc* metals. The main component detected is $F = \{110\}\langle 100 \rangle$, typical for ordered metals with B2 structure, like NiAl [24]. Taking both texture components possible interphase orientation relationships are:

$$\begin{aligned} \{100\}_{fcc} \parallel \{110\}_{bcc}, \langle 110 \rangle_{fcc} \parallel \langle 100 \rangle_{bcc} \\ \{110\}_{fcc} \parallel \{110\}_{bcc}, \langle 110 \rangle_{fcc} \parallel \langle 100 \rangle_{bcc} \\ \{110\}_{fcc} \parallel \{100\}_{bcc}, \langle 100 \rangle_{fcc} \parallel \langle 110 \rangle_{bcc}. \end{aligned}$$

The orientation relationship between two main shear components for *fcc* and *bcc* metals (C and F) is shown in Fig. 6. The obtained results also show that the addition of 0.05 at.% B was not sufficient to suppress the stress-induced formation of the incoherent NiAl-B2 phase.

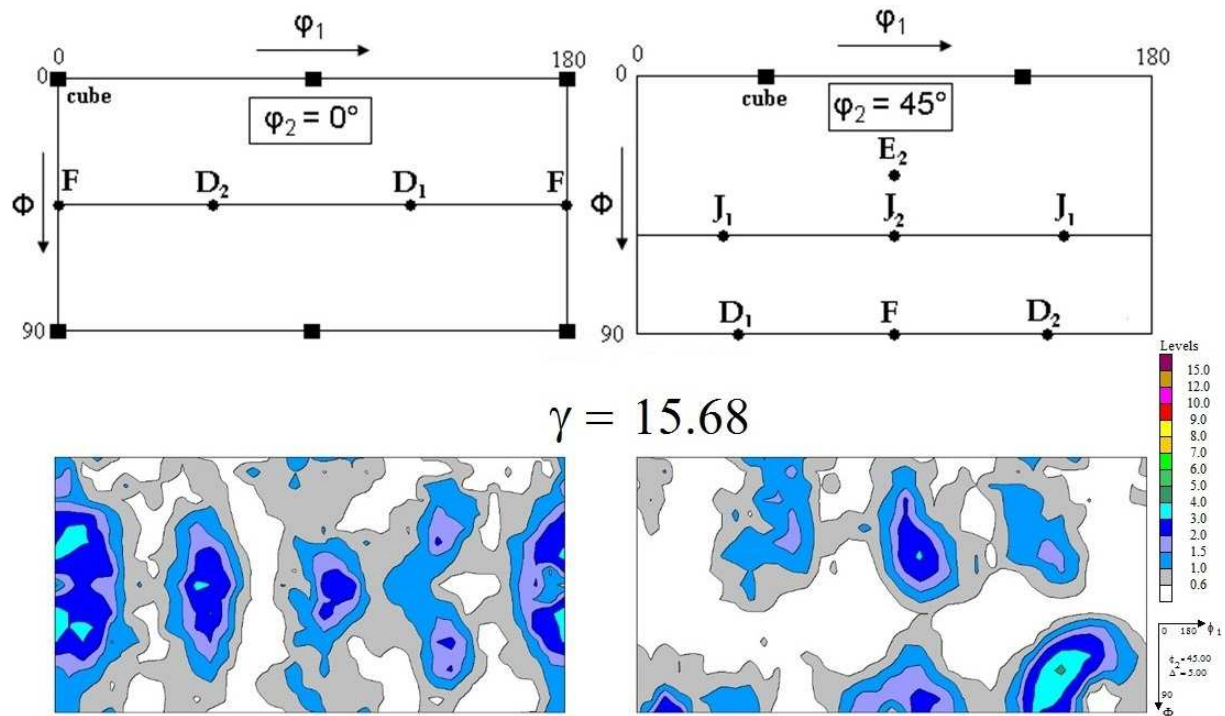


Fig. 5: ODF sections at $\phi_2 = 0^\circ$ and 45° after HPT of the NiAl-B2 phase at a shear strain of 15.68. Key figures give the ideal components of simple shear of *bcc* metals.

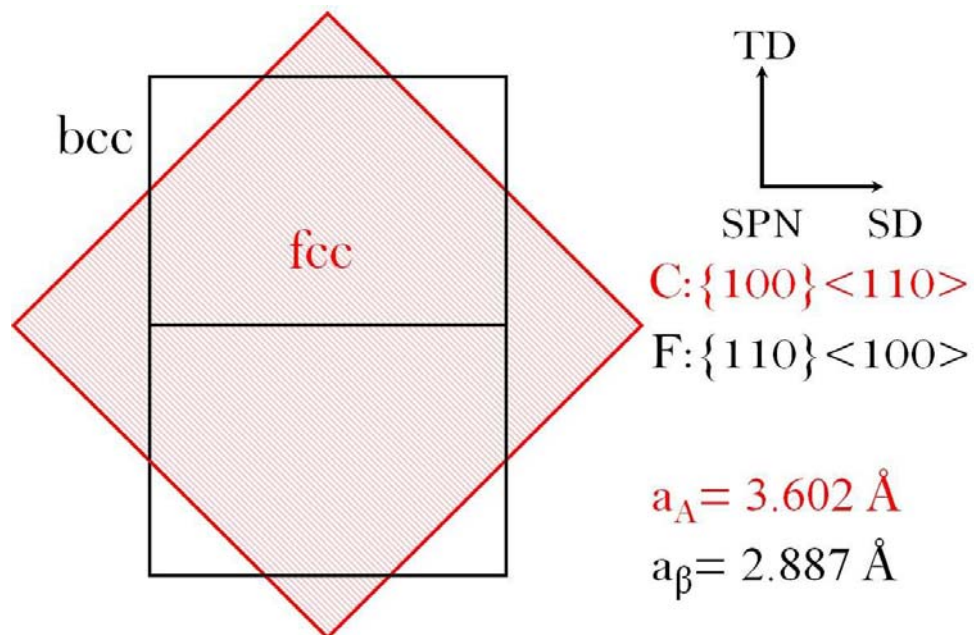


Fig. 6: Orientation relationship between two main texture components (C and F) for *fcc* (red) and *bcc* (black) metals. Lattice parameters determined by synchrotron X-ray diffraction.

4. Conclusions

The results of HPT-processed Fe-based alloys can be summarized as follows:

1. HPT-processing at room temperature leads to an intensive precipitation of NiAl-B2 phase.
2. The texture of HPT-processed Fe-based alloys is characterized by a strong C component for the austenitic phase and a strong F component for NiAl-B2 precipitates. These may give rise to certain interphase orientation relationships.
3. The texture components observed are typical for *fcc* metals with high stacking fault energy and for *bcc* metals of ordered B2 structure.
4. The addition of boron by 0.05 at.% does not suppress the formation of NiAl-B2 phase.

Acknowledgment

The financial support of the National Science Centre of Poland through project 2014/13/D/ST8/03108 is acknowledged.

References

- [1] Tanaka Y, Himuro Y, Kainuma R, Sutou Y, Omori T and Ishida K 2010 *Science* **327** 1488
- [2] Omori T, Ando K, Okano M, Xu X, Tanaka Y, Ohnuma I, Kainuma R and Ishida K 2011 *Science* **333** 68
- [3] Roy AK and Venkatesh A 2010 *J. Alloys Comp.* **577** 393
- [4] Chumlyakov YI, Kireeva I, Kretinina I, Kuts I, Kejnih OA, Kirillov KS, Karaman I, Maier I and Karaka H Thermoelastic martensitic transformations into new high-strength FeNiCoAlX (X= Ta, Ti, Nb, B) single crystals. *Abstract Book*, ICOMAT (2014) Bilbao Spain
- [5] Hornbogen E, Meyer W 1967 *Acta Metall.* **15** 584
- [6] Maki T, in: Otsuka K, Wayman CW (Eds.) 1999 *Shape Memory Materials*, Cambridge University Press; Revised edition
- [7] Sehitoglu H, Karaman I, Zhang XY, Chumlyakov Y and Maier HJ 2001, *Scripta Mater* **44** 779
- [8] Kireeva IV, Chumlyakov YI, Kirillov VA, Karaman I and Cesari E 2011 *Tech. Phys. Lett.* **37** 86
- [10] Ma J, Kockar B, Evirgen A, Karaman I, Luo ZP and Chumlyakov YI 2012 *Acta Mater.* **60** 2186
- [11] Chumlyakov YI, Kireeva IV, Panchenko EY, Kirillov VA, Timofeeva EE, Kretinina IV, Danilson YN, Karaman I, Maier H and Cesari E 2012 *Russ. Phys. J.* **54** 937
- [12] Ma J, Hornbuckle BC, Karaman I, Thompson GB, Luo ZP and Chumlyakov YI, 2013 *Acta Mater.* **61** 344
- [13] Lee D, Omori T and Kainuma R 2014 *J. Alloys and Compd.* **617** 120
- [14] Tseng LW, Ma J, Karaman I, Wang SJ and Chumlyakov YI 2015 *Scripta Mater.* **101** 1
- [15] Chumlyakov YI, Kireeva IV, Kutz OA, Karaca HE and Karaman I 2016 *Scripta Mater.* **119** 43
- [16] Krooß P, Holzweissig MJ, Niendorf T, Somsen C, Schaper M, Chumlyakov YI and Maier HJ 2014 *Scripta Mater.* **81** 28
- [17] Tanaka Y, Kainuma R, Omori T and Ishida K 2015 *Mat. Today Proc.* **2S** 485
- [18] Pagounis E, Chulist R, Lippmann T, Laufenberg M and Skrotzki W 2013 *Appl. Phys. Lett.* **103** 111911
- [19] Chulist R, Straka L, Sozinov A, Lippmann T and Skrotzki W, 2013 *Scripta Mater.* **68** 671
- [20] Randau C, Garbe U and Brokmeier H-G 2011 *J. Appl. Crystallogr.* **44** 641
- [21] Pawlik K and Ozga P *Gottinger Arb. Geol. Palaont.* SB4 (1999) 146
- [22] Toth LS and Molinari A 1994 *Acta Metall.* **42** 2459
- [23] Chulist R, Skrotzki W, Oertel C-G, Bohm A, Brokmeier H-G and Lippmann T 2012 *Int. J. Mater. Res.* **103** 575
- [24] Tränkner C, Chulist R, Skrotzki W, Beausir B, Lippmann T, Horky J and Zehetbauer M 2014 *IOP Conf. Series Mat. Sci. Eng.* **63** 012154